Journal of Physiology (1992), **456**, *pp.* 405–424
With 11 *figures*
Printed in Great Britain

RESTING MEMBRANE POTENTIAL AND POTASSIUM CURRENTS IN CULTURED PARASYMPATHETIC NEURONES FROM RAT INTRACARDIAC GANGLIA

BY Z.-J. XU AND D. J. ADAMS*

From the Department of Molecular and Cellular Pharmacology, University of Miami School of Medicine, Miami, FL 33101, USA

(*Received 28 October 1991*)

SUMMARY

1. Whole-cell K^+ currents contributing to the resting membrane potential and repolarization of the action potential were studied in voltage-clamped parasympathetic neurones dissociated from neonatal rat intracardiac ganglia and maintained in tissue culture.

2. Rat intracardiac neurones had a mean resting membrane potential of −52 mV and mean input resistance of 850 MΩ. The current–voltage relationship recorded during slow voltage ramps indicated the presence of both leakage and voltage-dependent currents. The contribution of Na^+, K^+ and Cl^- to the resting membrane potential was examined and relative ionic permeabilities $P_{Na}/P_K = 0{\cdot}12$ and $P_{Cl}/P_K < 0{\cdot}001$ were calculated using the Goldman–Hodgkin–Katz voltage equation. Bath application of the potassium channel blockers, tetraethylammonium ions (TEA; 1 mM) or Ba^{2+} (1 mM) depolarized the neurone by ~ 10 mV. Inhibition of the Na^+–K^+ pump by exposure to K^+-free medium or by the addition of 0·1 mM ouabain to the bath solution depolarized the neurone by 3–5 mV.

3. In most neurones, depolarizing current pulses (0·5–1 s duration) elicited a single action potential of 85–100 mV, followed by an after-hyperpolarization of 200–500 ms. In 10–15% of the neurones, sustained current injection produced repetitive firing at maximal frequency of 5–8 Hz.

4. Tetrodotoxin (TTX; 300 nM) reduced, but failed to abolish, the action potential. The magnitude and duration of the TTX-insensitive action potential increased with the extracellular Ca^{2+} concentration, and was inhibited by bath application of 0·1 mM Cd^{2+}. The repolarization rate of the TTX-insensitive action potential was reduced, and after-hyperpolarization was replaced by after-depolarization upon substitution of internal K^+ by Cs^+. The after-hyperpolarization of the action potential was reduced by bath application of Cd^{2+} (0·1 mM) and abolished by the addition of Cd^{2+} and TEA (10 mM).

5. Depolarization-activated outward K^+ currents were isolated by adding 300 nM TTX and 0·1 mM Cd^{2+} to the external solution. The outward currents evoked by step depolarizations increased to a steady-state plateau which was maintained for > 5 s. The instantaneous current–voltage relationship, examined under varying external

* To whom correspondence should be addressed.

MS 9849

K^+ concentrations, was linear, and the reversal (zero current) potential shifted in accordance with that predicted by the Nernst equation for a K^+-selective electrode. The shift in reversal potential of the tail currents as a function of the extracellular K^+ concentration gave a relative permeability, $P_{Na}/P_K = 0{\cdot}02$ for the delayed outward K^+ channel(s).

6. The outward K^+ current was reduced by 35% when extracellular Ca^{2+} was replaced by Mg^{2+}, or when Cd^{2+} (0·1 mM) was added to the external solution. These data suggest that the outward K^+ current in rat parasympathetic cardiac neurones is comprised of at least two components: a voltage-dependent delayed rectifying K^+ current (I_{Kv}) and a Ca^{2+}-activated K^+ current (I_{KCa}). The macroscopic K^+ current showed no rapidly activating and inactivating component.

7. The activation kinetics of the outward K^+ current were voltage dependent, with the rate of activation increasing at more depolarized potentials. The half-time to peak K^+ current amplitude was reduced from 4·7 ms at 0 mV to 3·2 ms at +60 mV. The slow decline of the outward current amplitude during prolonged depolarization followed an exponential time course with a time constant of decay of approximately 10 s at +60 mV. This slow 'inactivation' of K^+ currents was accelerated by increasing depolarization.

8. The conductance–voltage relationship of the Ca^{2+}-insensitive K^+ current, I_{Kv}, was fitted by a Boltzmann equation with half-maximal activation (V_h) at +2·6 mV and a slope factor (k) of 18·6 mV. The steady-state inactivation curve for the I_{Kv} was fitted by a Boltzmann equation with V_h of −22·0 mV and k of 9·4 mV.

9. The delayed outward K^+ current was abolished upon replacement of internal K^+ with either Cs^+ or arginine. Bath application of TEA blocked the total and Ca^{2+}-insensitive K^+ currents in a reversible and dose-dependent manner with K_i values (concentrations producing 50% inhibition of maximum response) of 2·8 and 2·3 mM, respectively.

10. Bath application of charybdotoxin (CTX) inhibited the total outward K^+ current by ~35% and the remaining current was not further reduced by the addition of 0·1 mM Cd^{2+} to the bath solution. CTX (100 nM) selectively inhibited I_{KCa} in these neurones.

11. A maximally effective concentration of 4-aminopyridine (1 mM) inhibited the total outward K^+ current by 30% and produced a 4–5-fold increase in the half-time of activation. Bath application of 2 mM Ba^{2+} reversibly abolished I_{KCa} and inhibited I_{Kv} by ~70%.

12. We conclude that I_{Kv} and I_{KCa} contribute to the repolarization of the action potential and the after-hyperpolarization observed in rat intracardiac neurones and hence influence vagally mediated neurotransmission in mammalian cardiac ganglia.

INTRODUCTION

The extensive network of neuronal cell bodies receiving parasympathetic vagal input and comprising the intrinsic cardiac ganglia of the mammalian heart has been long known (Meiklejohn, 1914; Woollard, 1926), yet the precise function of the network and how it mediates vagal input is largely unknown. A detailed description of the location, distribution and projections of the intracardiac ganglia has been provided for the rat heart (King & Coakley, 1958; Ellison & Hibbs, 1976; Moravec

& Moravec, 1984; Pardini, Patel, Schmid & Lund, 1987). These ganglia could well represent the final common pathway through which the diverse, extrinsic neural signals to the heart are modified before being transmitted to the effector tissues.

Investigations of the electrical properties of parasympathetic neurones of intracardiac ganglia using intracellular recording techniques have been made in the amphibian preparations of the frog (Dennis, Harris & Kuffler, 1971) and mudpuppy, *Necturus maculosus* (Roper, 1976). The ionic currents underlying the action potential in parasympathetic cardiac neurones enzymatically isolated from the interatrial septum of bullfrog heart have recently been studied using the patch-clamp technique (Clark, Tse & Giles, 1990). Electrophysiological studies of isolated mammalian cardiac neurones are, however, more difficult because of their inaccessibility.

Extracellular recordings of neural activity from ganglionated plexi located on the atrial epicardium of the mammalian heart *in vivo* have been carried out in several laboratories (Nozdrachev & Pogorelov, 1982; Gagliardi, Randall, Bieger, Wurster, Hopkins & Armour, 1988; Armour & Hopkins, 1990). Recently, intracellular recordings have been made from cultured neurones from intracardiac ganglia obtained from the atria of the newborn guinea-pig heart (Allen & Burnstock, 1987) and in cardiac ganglion preparations *in situ* of the neonatal rat (Seabrook, Fieber & Adams, 1990) and dog (Xi, Thomas, Randall & Wurster, 1991). Intracellular microelectrode recordings from intracardiac neurones cultured from guinea-pig atria revealed the existence of three different types of neurones within the ganglia (Allen & Burnstock, 1987). However, a comprehensive study of the ionic conductances underlying neuronal excitability in mammalian parasympathetic cardiac ganglia is lacking.

This study examines the ionic basis of the resting membrane potential and voltage-sensitive K^+ currents in a preparation of cultured neurones dissociated from parasympathetic cardiac ganglia of neonatal rat atria.

METHODS

Cell isolation and tissue culture

Newborn rats, 3 to 7 days of age, were killed by cervical dislocation and decapitation prior to removal of the atria. A description of the procedure to locate and visualize intracardiac ganglia in the neonatal rat heart *in situ* has been published (Seabrook *et al.* 1990). A schematic diagram to illustrate the distribution of intracardiac ganglia in neonatal rat atria is shown in Fig. 1*A*. A photomicrograph of parasympathetic neurones of the neonatal rat cardiac ganglion in the living preparation is shown in Fig. 1*B*. The preparation of cultures of neurones from dissociated cells of the neonatal rat cardiac ganglion plexus has been described previously (Fieber & Adams, 1991). Briefly, atria were incubated in collagenase (1 mg/ml; Worthington-Biomedical, specific activity 201 units/ml) for 1 h at 37 °C, prior to individual ganglia being excised and dispersed by trituration in a high-glucose culture medium (Dulbecco's Modified Eagle Medium; GIBCO Laboratories, NY, USA) with the addition of 10% fetal calf serum, 100 units/ml penicillin and 0·1 mg/ml streptomycin. Dissociated cells were plated onto 18 mm glass coverslips coated with laminin and incubated at 37 °C in a 95% air, 5% CO_2 atmosphere. Three or four ganglia were dissected for each culture, which (with the approximately 20% survival rate and/or plating efficiency) resulted in 100–200 neurones per culture dish. Cultures were used between 24 and 72 h after plating, since by this time the neurones appeared to have recovered from enzyme treatment and were firmly attached to the coverslip. Figure 1*C* illustrates the morphology of the neurones at this stage. Experiments were carried out at room temperature (23 ± 2 °C).

Electrophysiological recording and data analysis

The electrical properties of cultured intracardiac ganglion cells were studied under current- and voltage-clamp modes using the whole-cell patch-clamp technique (Hamill, Marty, Neher, Sakmann & Sigworth, 1981). Pipettes (2–3 MΩ) were constructed from thin-walled borosilicate glass (Clarke

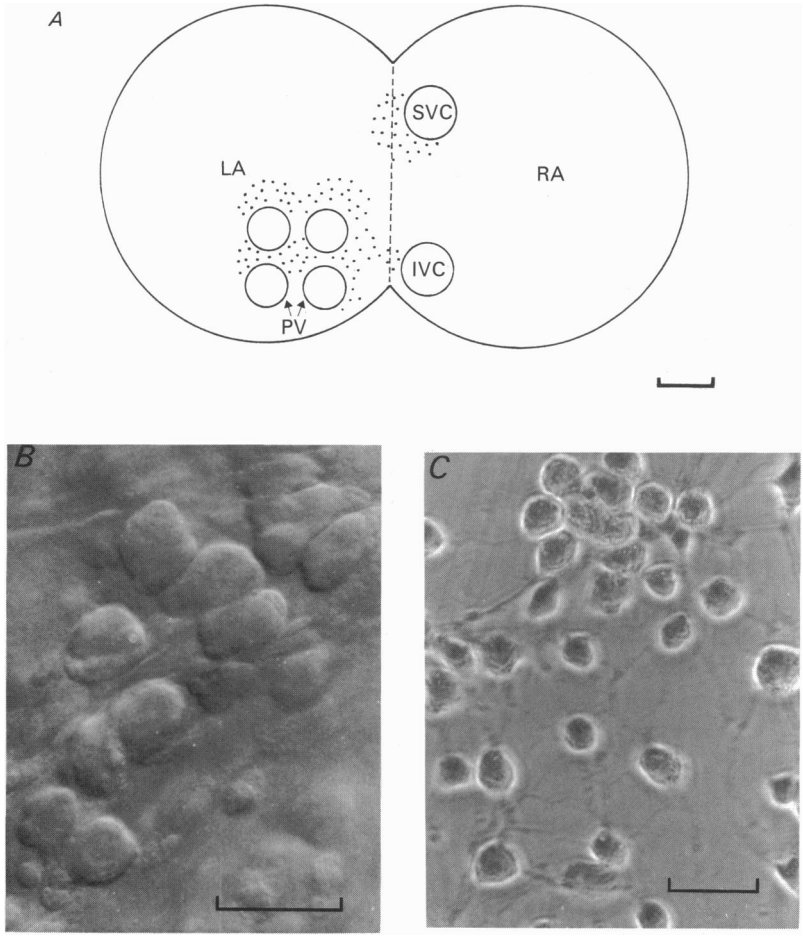

Fig. 1. Rat parasympathetic cardiac ganglia *in situ* and dissociated intracardiac neurones grown in tissue culture. *A*, distribution of intracardiac ganglia (stippled regions) on the epicardial surface of neonatal rat atria. LA, left atria; RA, right atria; SVC, superior vena cava; IVC, inferior vena cava; PV, pulmonary veins. Scale bar, 1 mm. *B*, intrinsic cardiac neurones in a living ganglion preparation viewed with Hoffman modulation contrast optics. Scale bar, 40 μm. *C*, phase-contrast photomicrograph of neurones dissociated from explants of rat cardiac ganglia and grown in tissue culture for 48 h. Neuronal soma (25–35 μm diameter) and axonal processes visualized at 400× magnification. Scale bar, 100 μm.

Electromedical, UK). Cells were viewed under phase-contrast optics at 400× magnification and seals (> 5 GΩ) were formed between the patch electrode and the soma membrane. The membrane under the electrode was ruptured with further suction to obtain the whole-cell recording configuration. The resting potential was measured immediately after achieving the whole-cell

configuration and at least 5 min was allowed for equilibration between the pipette solution and the cell to permit membrane conductances to stabilize. Voltage steps were applied in 10 mV increments from −100 mV with pulse protocols generated by a PC 80386 computer and pCLAMP programs (Axon Instruments Inc., CA, USA). Membrane capacitative and leak currents were subtracted digitally using a −P/4 pulse protocol. The use of the −P/4 protocol was based on a linear relationship between ionic current and membrane potential at voltages negative to −60 mV (see Fig. 3*A*). Indeed, in controls where voltage-dependent Na^+, Ca^{2+} and K^+ currents were inhibited, a linear 'leak' current–voltage relation was observed for a voltage ramp from −150 to +100 mV. Cell capacitance (C_m) and series resistance (R_s), determined for each cell from the compensation of the capacity transient in response to a −10 mV voltage step, were 19±5 pF and 5·2±1·7 MΩ (mean±S.D., $n = 60$), respectively. Fifty to sixty per cent of the measured R_s was compensated in most experiments, however, an uncompensated R_s of 2 MΩ would produce a voltage error of 10 mV for a whole-cell current of 5 nA amplitude. Membrane voltage and current were recorded with a List LM/EPC-7 patch-clamp amplifier, filtered at 10–30 kHz (−3 dB, 4-pole Bessel Filter; Ithaco 4302), digitized at 50 kHz using an analog-to-digital interface (12-bit resolution; Tecmar Labmaster TM 125 – DMA) and stored for later analysis. Membrane voltage and holding current were monitored continuously throughout the experiment on a chart recorder (Soltec 1242).

For experiments investigating the actions of channel blockers, it was assumed that the interaction between the ion channel and blocker (B) obeyed the law of mass action. The peak amplitude of the current obtained in the presence of the blocker (I) was normalized against the amplitude of the current obtained in the absence of the blocker (I_{max}). Dose–response curves were fitted according to the equation,

$$I = I_{max}/(1+([K_i]/[B])^{n_H}), \quad (1)$$

where K_i is the concentration of blocker that produces 50% inhibition of the maximum response, and n_H is a factor that describes the steepness of the dose–response curve usually termed the Hill coefficient.

All numerical data are represented as means±standard error of the mean (S.E.M.).

Solutions and chemicals

The extracellular physiological salt solution (PSS) used during electrical recordings contained (mM): 133 NaCl, 4·7 KCl, 2·5 $CaCl_2$, 0·6 $MgCl_2$, 7·7 D-glucose, 10 HEPES, adjusted to pH 7·4 with NaOH. The recording chamber (~0·3 ml volume) was continually perfused at 0·5–1 ml/min. Patch pipettes were filled with an intracellular solution containing 130 mM KCl, 0·1–1 mM K_2EGTA or K_4BAPTA, 2 mM MgATP, and 10 mM HEPES-KOH; pH 7·2 at 22 °C. In one series of experiments, NaCl was replaced isosmotically by arginine chloride and $CaCl_2$ by $MgCl_2$. Changes in the extracellular K^+ concentration were made by isosmotic substitution of NaCl for KCl. The osmotic activity (270–280 mmol/kg) of the solutions was monitored with a vapour pressure osmometer (Wescor 5500). Corrections for liquid junction potentials between the bath solution and indifferent electrode (0·15 M KCl agar bridge) were made with respect to a reference electrode (saturated KCl, reverse sleeve junction; Corning X-EL 47619).

All solutions were made using analytical grade reagents. Arginine chloride, ethyleneglycol-bis-(β-aminoethylether) *N,N,N′,N′*-tetraacetic acid (EGTA), tetraethylammonium chloride (TEACl), $BaCl_2$ and laminin were obtained from Sigma Chemical Co. (St Louis, MO, USA), $CdCl_2$, CsCl and 4-aminopyridine (4-AP) from Aldrich Chemical Co. (Milwaukee, WI, USA), 1,2-bis(2-amino-phenoxy)ethane-*N,N,N′,N′*-tetraacetic acid (BAPTA) from Molecular Probes Inc. (Eugene, OR, USA), tetrodotoxin (TTX) from Calbiochem Corp. (San Diego, CA, USA) and charybdotoxin (CTX) from Peptides International (Louisville, KY, USA).

RESULTS

Cultured parasympathetic neurones dissociated from explants of rat cardiac ganglia were spherical with diameters ranging from 25 to 35 μm. Axonal processes originating from the cell soma indicated that these neurones were usually uni- or bipolar (see Fig. 1*C*). Clusters of three to ten cells were often observed in the cultures,

but only isolated neurones capable of generating an action potential in response to injected depolarizing current pulses were studied electrophysiologically. Results from > 270 such neurones are described.

Passive membrane properties

Passive and active electrical properties of isolated cardiac neurones were examined under current clamp and used for comparison with conventional microelectrode

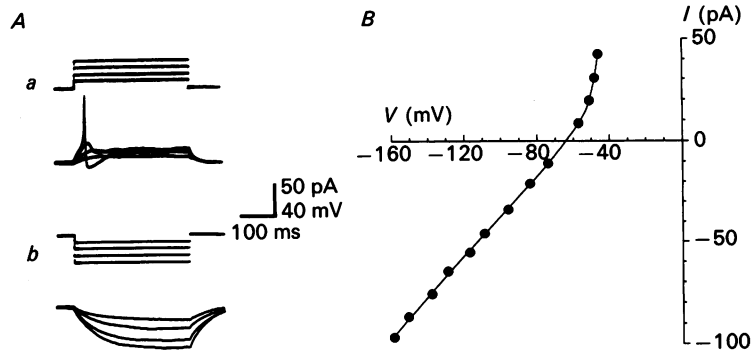

Fig. 2. Passive electrical properties of cultured rat intracardiac neurones. *A*, electrotonic voltage responses to (*a*) depolarizing and (*b*) hyperpolarizing current pulses. Depolarizing current pulses (> 40 pA) evoked action potentials that had a threshold of about −45 mV and a peak amplitude > 80 mV. *B*, current–voltage relationship of an isolated neurone in physiological salt solution. The steady-state voltage was measured in response to a 300 ms constant current pulse applied at the resting membrane potential (−64 mV).

records from other autonomic ganglion cells. The cardiac ganglion cells had resting membrane potentials ranging from −45 to −65 mV (−52±2·1 mV, $n = 26$) and an average input resistance of 850±23 MΩ ($n = 24$). The electrotonic response of a typical intracardiac neurone to hyperpolarizing and depolarizing constant current pulses is shown in Fig. 2*A*. The specific membrane resistance calculated from the time constant of the cell ($\tau = R_m C_m$ where $C_m = 1\ \mu F/cm^2$) obtained at −60 mV was ~ 50 kΩ cm². The whole-cell *I–V* relationship is linear at membrane potentials negative to the resting potential indicating a voltage-independent 'leakage' current (Fig. 2*B*).

The relationship between extracellular [K^+] and resting membrane potential was examined in these neurones. In Fig. 3*A* the whole-cell current–voltage (*I–V*) relationship was monitored using an experimental protocol in which the voltage was slowly ramped (4 s) from −150 to +30 mV. Depolarization-activated Na^+ and Ca^{2+} currents were inactivated due to the slow time course of the depolarizing voltage ramp (Xu & Adams, 1992). Increasing the extracellular [K^+] shifted the *I–V* curves to more positive potentials and in the presence of isotonic KCl (150 mM), an inward current was observed at negative potentials due to the electrochemical gradient for K^+ movement through open K^+ channels. Figure 3*B* plots mean resting potential as a function of the extracellular [K^+]. The smooth curve was obtained by fitting the data with the Goldman–Hodgkin–Katz (GHK) constant-field equation (Goldman,

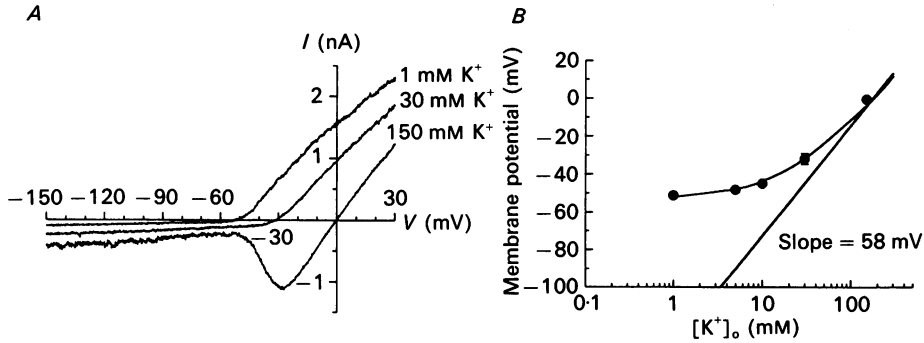

Fig. 3. *A*, current–voltage relationships obtained by applying a 4 s voltage ramp from −150 to +30 mV in the presence of 1, 30 or 150 mM extracellular K^+ in the same neurone. *B*, resting membrane potentials (zero holding current) are plotted as a function of the extracellular K^+ concentration (logarithmic scale). ● represents the mean ± S.E.M. values of resting membrane potentials determined in four cells. The data were fitted with GHK voltage equation (smooth curve) with $P_{Na}/P_K = 0{\cdot}12$. The straight line was drawn according to the Nernst equation for a K^+-selective electrode with a slope of 58 mV.

TABLE 1. Resting membrane potentials of cultured rat intracardiac neurones measured in different extracellular solutions

External solution	Resting membrane potential (mV)	*n*
Normal PSS (control)	−52·5 ± 2·1	26
Na^+-free (arginine) PSS	−65·6 ± 3·0*	6
Ca^{2+}-free (Mg^{2+}) PSS	−52·3 ± 0·5	3
Cl^--free (aspartate) PSS	−53·5 ± 0·6	3
PSS + 1 mM TEA	−42·3 ± 1·0*	3
PSS + 1 mM Ba^{2+}	−39·5 ± 2·3*	4
PSS + 0·1 mM ouabain	−49·2 ± 1·5	5

* Level of significance, $P < 0{\cdot}05$.

1943; Hodgkin & Katz, 1949). The relative permeabilities to Na^+ (P_{Na}/P_K) and Cl^- (P_{Cl}/P_K) obtained from the curve fitting are 0·12 and < 0·001, respectively, indicating that the neuronal membrane has relatively high resting Na^+ permeability and that Cl^- is not significantly permeant (see Table 1). The straight line in Fig. 3*B* is drawn according to the Nernst equation with a slope of 58 mV/10-fold change in extracellular [K^+]. The data points deviate from the limiting slope at K^+ < 30 mM, indicating that both Na^+ and K^+ contribute to the resting membrane potential.

The ionic basis of the resting membrane potential was further investigated by substituting relatively large, 'impermeant' ions for the physiological extracellular cations and anions (Table 1). Isotonic replacement of extracellular NaCl with arginine chloride hyperpolarized the neurone by 13 ± 3 mV ($n = 6$), consistent with the prediction of the GHK equation with the relative Na^+ permeability given above. This hyperpolarization was accompanied by a decrease in the holding current at −70 mV. Isotonic replacement of extracellular Cl^- with aspartate hyperpolarized the cell by 1·5 ± 0·6 mV ($n = 3$), an effect which may be due to a decrease in the extracellular Na^+ activity.

Contribution of a K^+ conductance to the resting membrane potential is further supported by the effects of K^+ channel blockers: bath application of PSS containing either 1 mM TEACl or 1 mM $BaCl_2$ depolarized the neurone by 10 ± 1 mV ($n = 3$) and $13 \pm 2{\cdot}3$ mV ($n = 4$), respectively, and decreased the whole-cell outward current. Replacement of external Ca^{2+} by Mg^{2+} or raising the intracellular BAPTA concentration (10 mM) did not change the resting membrane potential suggesting that a Ca^{2+}-activated K^+ conductance activated at rest does not contribute to the resting membrane potential. Inhibition of the Na^+–K^+ pump by exposure to K^+-free external solution or by addition of ouabain (0·1–1 mM) in the bath depolarized the neurone by 3–5 mV, suggesting that active Na^+ and K^+ transport makes only a minor electrogenic contribution to the resting membrane potential. Taken together, these data suggest that the resting membrane potential of these neurones is determined primarily by a resting permeability to K^+ and to a lesser extent Na^+. Na^+–K^+ pump activity and resting membrane Cl^- permeability make only minor contributions to the resting membrane potential.

Action potentials in cultured neurones

Although cultured neurones were not spontaneously active, brief depolarizing current pulses elicited overshooting action potentials, which had a mean threshold of -40 mV and an amplitude of 80–105 mV (Fig. 4*A*). Action potentials were followed by an after-hyperpolarization lasting 200–500 ms whose amplitude varied as a linear function of the membrane potential between -50 and -110 mV (not shown). The reversal potential of the after-hyperpolarization in normal PSS was $-76 \pm 1{\cdot}3$ mV ($n = 6$), compared to the calculated K^+ equilibrium potential (-85 mV). These parasympathetic neurones could follow brief (2–5 s) repetitive trains of current pulses at frequencies of up to 20 Hz. In response to 0·5–1 s depolarizing currents approximately 85% of the cells produced only a single action potential regardless of the stimulus intensity or duration. In the remaining 15% of neurones, sustained depolarizing current injection elicited repetitive firing with a maximal frequency of 5–8 Hz (Fig. 4*B*). An after-hyperpolarization was usually observed following both single action potentials and a burst of action potentials.

The relative contribution of Na^+ and Ca^{2+} ions to the action potential was assessed using sodium and/or calcium channel antagonists. Addition of 300 nM TTX to the bathing solution reduced the overshoot but failed to abolish the action potential. This concentration of TTX completely and reversibly blocks the voltage-dependent Na^+ conductance in these neurones (Xu & Adams, 1992). The TTX-insensitive action potential had a slower rate of rise than the control. The magnitude and duration of the regenerative response in TTX was increased by increasing extracellular [Ca^{2+}] to 10 mM or by replacing intracellular K^+ with Cs^+ (Fig. 4*C*). Addition of 0·1 mM $CdCl_2$ to the bath reversibly abolished the TTX-insensitive action potential. In contrast, extracellular Cd^{2+} reversibly reduced the overshoot of the action potential evoked in normal PSS by approximately 15%. In the presence of TTX and internal Cs^+, the action potential exhibited a plateau followed by a slow repolarization, and the after-hyperpolarization seen in PSS was replaced by a prolonged after-depolarization (Fig. 4*C*). The rate of repolarization of the action potential and the amplitude of the after-hyperpolarization in PSS were depressed by external TEA or Ba^{2+}. The after-hyperpolarization was inhibited by ~ 50% by bath application of 0·1 mM Cd^{2+} and

was further reduced by the addition of TEA (10 mM) to the external solution (Fig. 4*D*). These results suggest that the influx of Na^+ and Ca^{2+} contribute to the rising phase and overshoot of the action potential, and that the repolarization and after-hyperpolarization are mainly due to K^+ efflux. Membrane Na^+ and Ca^{2+} currents in

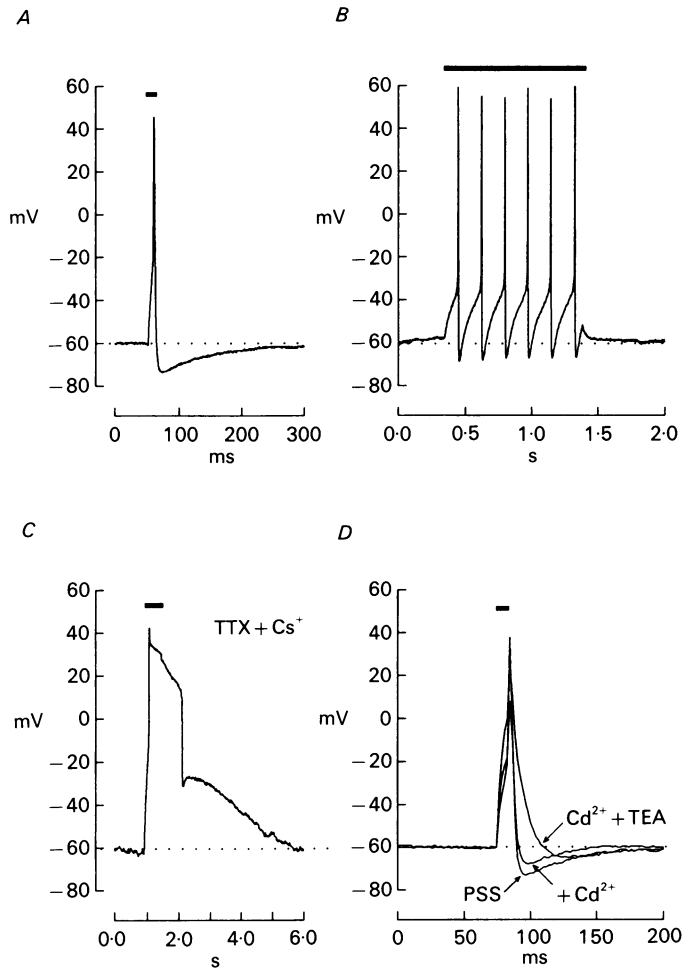

Fig. 4. Action potentials in cultured rat parasympathetic cardiac neurones. *A*, action potential elicited in response to a depolarizing current pulse (40 pA, 0·5 s) in normal PSS and internal KCl pipette solution. *B*, train of action potentials evoked in response to constant current injection (1 s duration) in normal PSS. *C*, calcium-dependent action potential evoked by current injection (40 pA), obtained in normal PSS containing 300 nM TTX and an internal CsCl pipette solution. *D*, superimposed traces of action potentials obtained in normal PSS, PSS containing 0·2 mM Cd^{2+}, and PSS containing 0·2 mM Cd^{2+} and 10 mM TEA. Resting membrane potentials: −60 mV in *A*, *B*, *C* and *D*.

cultured rat intracardiac neurones are characterized in the companion paper (Xu & Adams, 1992).

Depolarization-activated outward K^+ currents

The carrier of the delayed outward current was verified by examining tail currents obtained upon repolarization to a variable final voltage following a brief (15 ms) step

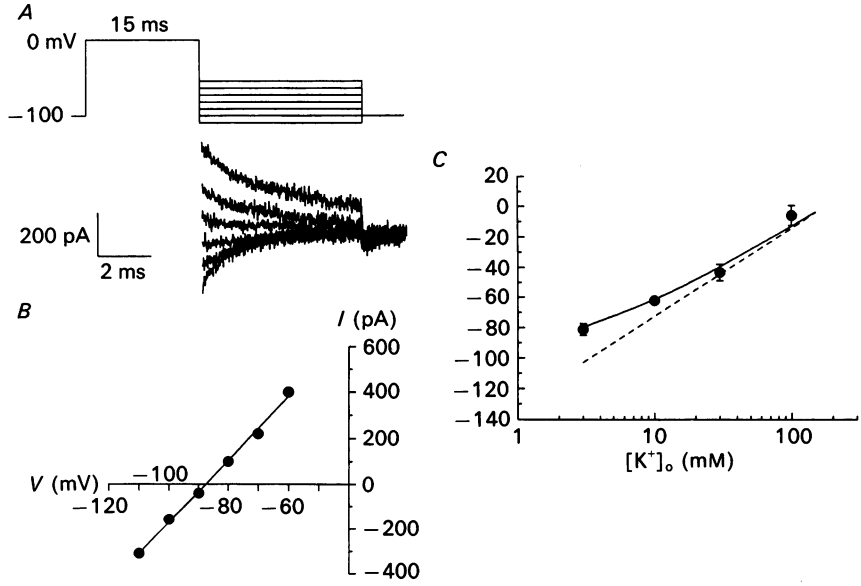

Fig. 5. The reversal potential for instantaneous tail currents as a function of extracellular $[K^+]$. *A*, tail currents elicited upon repolarization from 0 mV to membrane potentials from −60 to −110 mV. Bath solution contained 3 mM K^+. Holding potential = −100 mV. *B*, instantaneous *I–V* relationship for the delayed outward current. A linear regression line was fitted to the data (continuous line). *C*, the relationship between the reversal potential for the instantaneous tail currents and extracellular $[K^+]$. The data represent the mean values of the reversal potentials determined from three cells and are best fitted by the GHK equation with $P_{Na}/P_K = 0{\cdot}02$ (continuous line). The Nernst relation predicted for a K^+-selective electrode is shown by the dashed line.

to 0 mV. Instantaneous current amplitude plotted as a function of the final voltage reversed near −88 mV, close to the calculated K^+ equilibrium potential (Fig. 5). Elevation of bath $[K^+]$ reduced the steady-state outward current and shifted the reversal potential for tail currents to a more positive potential (Fig. 5*C*). This dependence of current amplitude and reversal potential on extracellular $[K^+]$ is consistent with K^+-selective channels underlying the delayed outward currents. Figure 5*C* plots reversal potentials recorded as a function of extracellular $[K^+]$. The deviation from the Nernst relation expected for a K^+-selective electrode (dashed line) was consistent with a small Na^+ permeability in the underlying channels (P_{Na}/P_K = 0·02; continuous line). Thus the delayed outward currents activated by depolarization are more K^+ selective than the resting membrane potential.

In normal PSS containing TTX (300 nM), outward currents evoked by depolarizing steps exhibited a time-dependent increase to a steady-state plateau (Fig. 6*A*). The

final magnitude of this delayed outward current varied between neurones; the current density at +90 mV averaged 542±55 pA/pF ($n = 8$). Depolarization-activated outward currents evoked after replacing Ca^{2+} with Mg^{2+} were smaller in amplitude by one-third at the most positive potentials (Fig. 6*B*). Steady-state

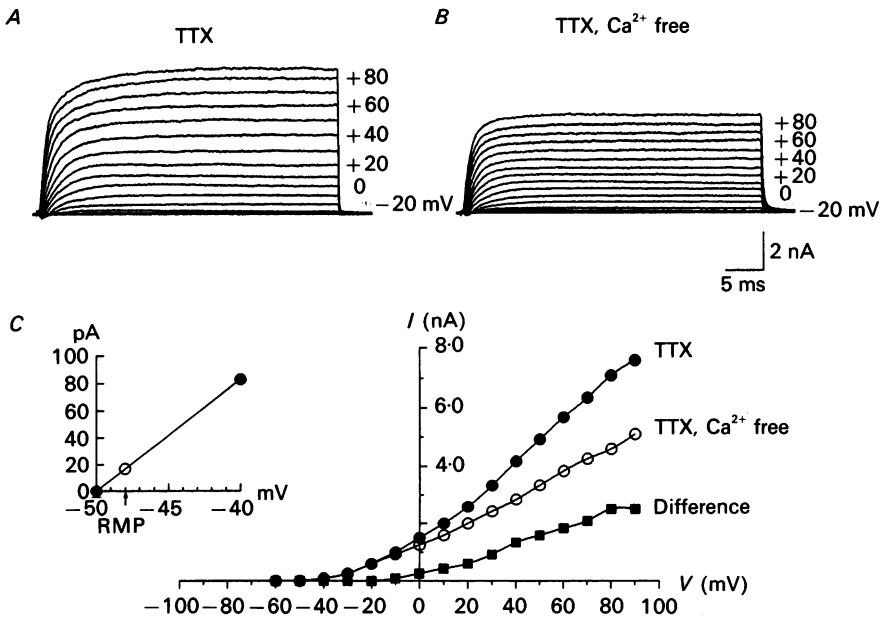

Fig. 6. Effects of TTX and Ca^{2+}-free medium on voltage-dependent ionic currents. *A*, membrane current elicited in response to 40 ms depolarizing voltage steps ranging from −60 to +90 mV in 10 mV increments from a holding potential of −100 mV in PSS containing 300 nM TTX. *B*, delayed outward currents obtained in 300 nM TTX with bath Ca^{2+} replaced by Mg^{2+}. *C*, *I–V* curves for delayed outward currents obtained in TTX in the presence (●) and absence (○) of bath Ca^{2+}, and the difference currents (■). Inset: amplified *I–V* relation for total I_K between −40 and −50 mV. Resting membrane potential, RMP = −48 mV.

current–voltage relations recorded in the presence (control) and absence (Ca^{2+} free) of external Ca^{2+} are shown in Fig. 6*C*. The 'difference' *I–V* relation represents the Ca^{2+}-sensitive outward current, which is activated at membrane potentials positive to −10 mV. Similar results were obtained upon addition of 0·1 mM $CdCl_2$ to the extracellular solution, suggesting that Ca^{2+} influx mediates the activation of the difference current. Hence, the delayed outward current of rat parasympathetic neurones is comprised of at least two components: a voltage-gated delayed rectifying K^+ current (I_{Kv}) and a Ca^{2+}-activated K^+ current (I_{KCa}).

Time and voltage dependence of I_{Kv} and I_{KCa}

The rate of activation of the outward K^+ current increased at more depolarized potentials. The time course of activation of the outward K^+ current was not well fitted by a single exponential function and thus was measured as the half-time ($t_{\frac{1}{2}}$) to peak current amplitude (Fig. 7*A*). Figure 7*B* plots $t_{\frac{1}{2}}$ as a function of membrane

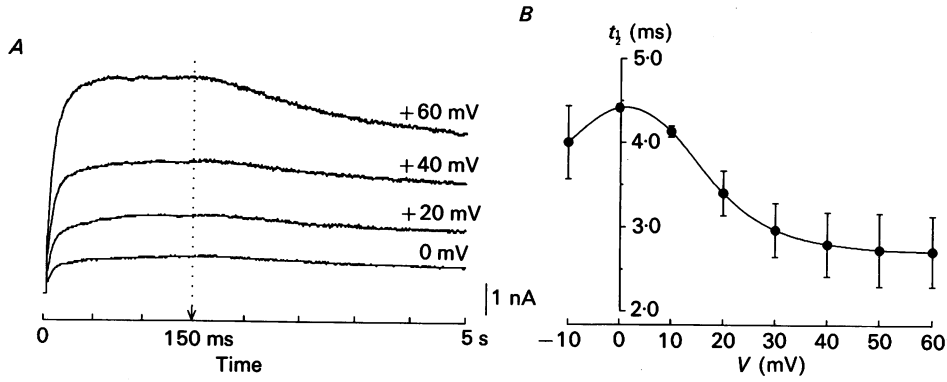

Fig. 7. Kinetics of activation and inactivation of the delayed K^+ current. *A*, superimposed records of delayed K^+ currents elicited by step depolarizations (5 s) to 0, +20, +40 and +60 mV from −100 mV. Delayed K^+ currents were recorded at two different sampling rates: 150 μs/point for the first 150 ms and then at 5 ms/point for the following 4·85 s. The transition is indicated by the dotted line. *B*, the half time ($t_{\frac{1}{2}}$) of activation of the delayed K^+ current plotted as a function of membrane potential. Points plot mean values for $t_{\frac{1}{2}}$ measured in three different cells.

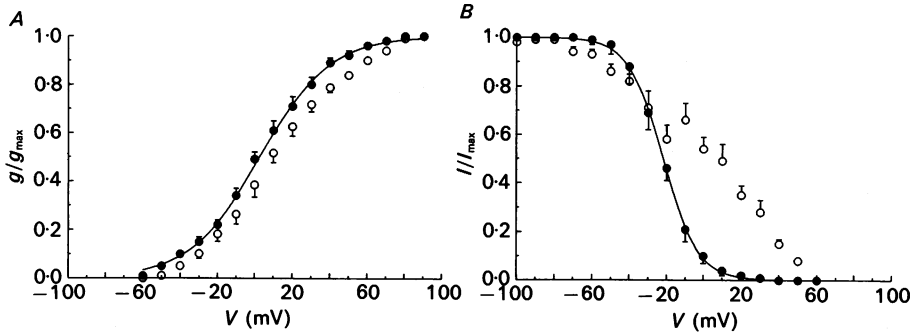

Fig. 8. Voltage dependence of activation and inactivation of the delayed K^+ conductance. *A*, voltage dependence of activation of the total and Ca^{2+}-insensitive K^+ conductance (g_K), determined from the *I–V* relationships measured in the presence of 30 mM K^+ and normalized to the maximal K^+ conductance ($g_{K(max)}$) for three cells. The conductance–voltage relationship for I_{Kv} (●) was fitted by the Boltzmann equation with $V_h = +2{\cdot}6$ mV and $k = 18{\cdot}6$ mV (continuous line). ○ represents the conductance–voltage relationship for the total outward K^+ current. *B*, voltage dependence of steady-state inactivation of the total and Ca^{2+}-insensitive delayed K^+ currents. The steady-state inactivation curve was determined from the K^+ current amplitude evoked by a +60 mV, 50 ms pulse from a variable 10 s holding potential and normalized to the maximum K^+ current obtained from a holding potential of −120 mV (I/I_{max}). The normalized Ca^{2+}-insensitive K^+ current (●) recorded in Cd^{2+} and determined from four cells was fitted by eqn (3) (continuous line). ○ represents the steady-state inactivation curve obtained for the normalized total outward K^+ current.

potential in three cells. Figure 7*A* also shows that the outward current declined during prolonged depolarization (5 s). This decline of the current followed an exponential time course with a time constant of decay of approximately 10 s at

+60 mV. This time constant decreased with increasing depolarization. This gradual fall in K^+ current might have been due to inactivation of the underlying conductance and/or to a reduction in the driving force due to K^+ accumulation in the extracellular space.

Extracellular [K^+] was raised to 30 mM to minimize the effects of the uncompensated series resistance and K^+ accumulation in the unstirred layer adjacent to the soma membrane. This elevation of bath [K^+] reduced the steady-state outward current and shifted the reversal potential for tail currents to a more positive potential (−45 mV; Fig. 5*C*). The steady-state K^+ current density measured in the presence of 30 mM K^+ was 352±67 pA/pF at +90 mV ($n = 6$). The relative conductance (g_K) of the total outward K^+ current and Ca^{2+}-insensitive K^+ current, I_{Kv}, was calculated from $I_K/(V-E_K)$, where I_K is the peak K^+ current amplitude and E_K is the K^+ equilibrium potential determined from the reversal potential of K^+ tail currents. The average conductance–voltage relationships for I_{Kv} determined from three cells (Fig. 8*A*) was fitted by the Boltzmann distribution:

$$g_K = g_{K(max)}/\{1+\exp[(V_h-V)/k]\}, \quad (2)$$

where g_K is the K^+ conductance at membrane potential, V. The maximum K^+ conductance, $g_{K(max)}$, is 17·0±1·3 nS; V_h, the voltage at which g_K is half-maximal is +2·6 mV and k, the slope factor, is 18·6 mV. The total outward K^+ current exhibited a similar conductance–voltage relationship (○ in Fig. 8*A*) with a maximum conductance of 25·4±4·5 nS ($n = 6$).

Inactivation of the delayed K^+ current was investigated by holding the cell for 10–30 s at different membrane potentials and then assessing the available K^+ current with a 50 ms step to +60 mV. The steady-state inactivation curve was determined by dividing the peak current at each holding potential by the peak current (I_{max}) generated from a holding potential of −120 mV. Figure 8*B* plots these normalized currents as a function of the holding potential, averaged from four cells. The steady-state inactivation curve for I_{Kv}, isolated from the total K^+ current by bath application of 0·1 mM Cd^{2+}, is described by the continuous line which represents a least-squares fit of the data according to the equation:

$$I/I_{max} = 1/\{1+\exp[(V-V_h)/k]\}, \quad (3)$$

where V_h is the potential at which I/I_{max} is 0·5 and k defines the slope. The average values for V_h and k were −22·0 and 9·4 mV, respectively. The steady-state inactivation curve for the total outward K^+ current (○ in Fig. 8*B*) exhibited a shallow voltage dependence and was fitted by eqn (3) with parameters $V_h = -1$ mV and $k = 26$ mV.

Pharmacological blockers of outward K^+ currents

The delayed outward current was completely abolished by replacement of internal K^+ with either Cs^+ or arginine, indicating that the outward current is carried by K^+. The sensitivity of the delayed outward K^+ currents to TEA was determined in the presence and absence of external Cd^{2+} (0·1 mM, Fig. 9*A*). Dose-dependent inhibition of the total delayed outward current and of the Cd^{2+}-insensitive component by the addition of TEA to the bath is shown in Fig. 9*A*. The averaged dose–response

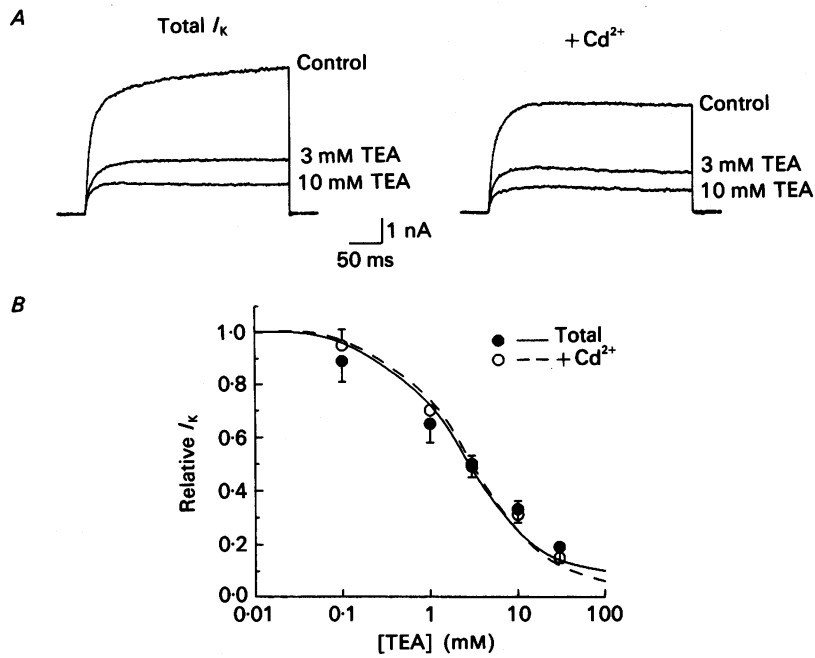

Fig. 9. Inhibition of total and Ca^{2+}-insensitive delayed K^+ currents by external TEA. *A*, superimposed traces of the total delayed outward K^+ current (left) and Cd^{2+}-insensitive component of the outward K^+ current (right) obtained in the absence and presence of 3 and 10 mM TEA. Outward K^+ currents were elicited by depolarizing voltage steps to +80 mV from a holding potential of −100 mV. *B*, dose–response relationship for TEA inhibition of delayed outward K^+ currents in the absence (●) and presence (○) of extracellular Cd^{2+}. Continuous and dashed lines show best fits by eqn (1) with K_i of 2·8 and 2·3 mM for the total and Ca^{2+}-insensitive delayed outward K^+ currents, respectively.

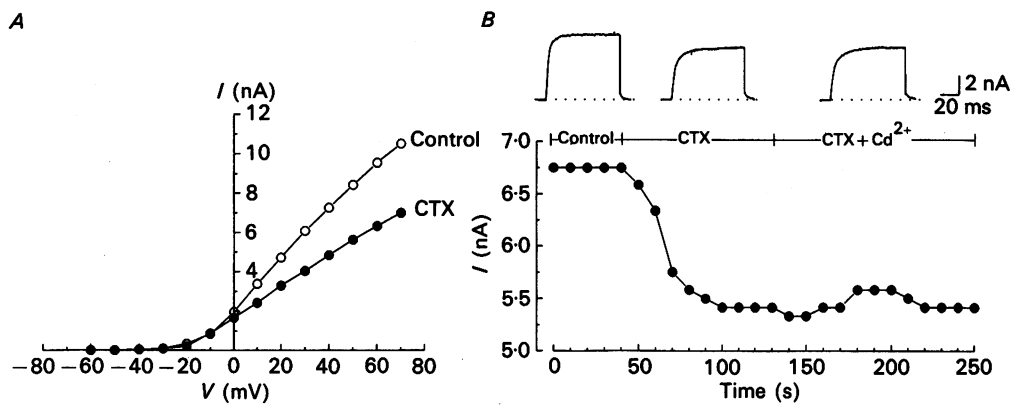

Fig. 10. Block of Ca^{2+}-dependent K^+ currents, I_{KCa}, by charybdotoxin (CTX). *A*, current–voltage relationships of the total outward K^+ current before and after bath application of 100 nM CTX. *B*, time course of inhibition of the outward K^+ current during superfusion with PSS containing 100 nM CTX and with PSS containing 100 nM CTX and 0·1 mM Cd^{2+}. Records of outward K^+ currents evoked by step depolarization to +40 mV from −100 mV were obtained in normal PSS (control), in the presence of CTX alone and CTX plus Cd^{2+}.

relations determined for depolarizations to +80 mV from a holding potential of −100 mV are shown in Fig. 9*B*. Averages from three to seven cells were fitted by eqn (1), assuming one TEA binding site per K^+ channel ($n_H = 1$), with K_i values for TEA inhibition of total and voltage-dependent I_K of 2·8 and 2·3 mM, respectively.

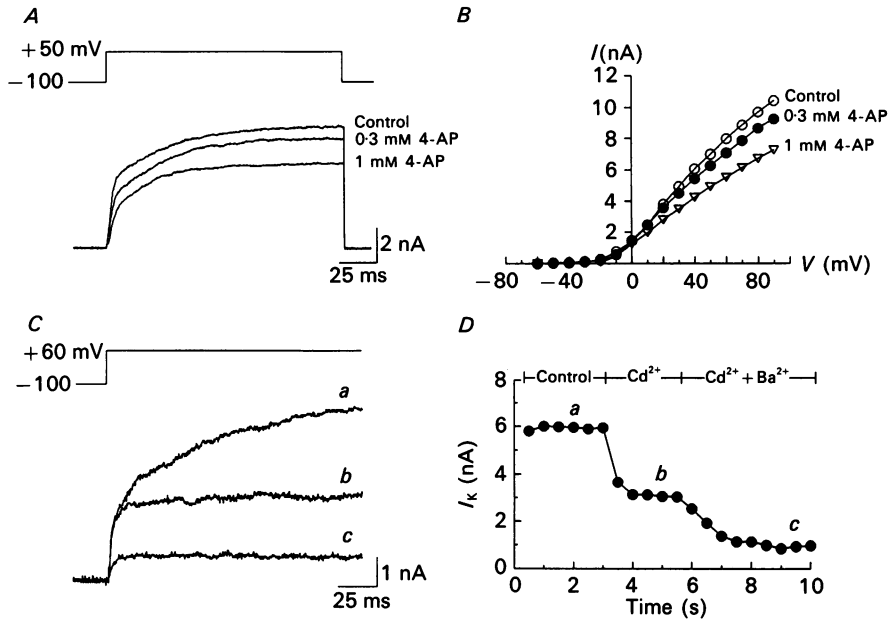

Fig. 11. Effects of 4-aminopyridine (4-AP) and Ba^{2+} on the delayed outward K^+ current. *A*, superimposed traces of total delayed outward K^+ currents obtained in the absence (control) and presence of 0·3 and 1 mM 4-AP. Currents were elicited by 200 ms depolarizing steps to +50 mV from a holding potential of −100 mV. *B*, delayed K^+ current–voltage relations obtained in the same neurone in the absence (control, ○) and presence of 0·3 (●) and 1 mM 4-AP (▽). *C*, superimposed traces of outward K^+ currents elicited by step depolarization to +60 mV from a holding potential of −100 mV in normal PSS (*a*) and in the presence of either 0·1 mM Cd^{2+} (*b*) or both Cd^{2+} and 2 mM Ba^{2+} (*c*). *D*, peak K^+ current amplitude evoked by the pulse protocol described above during sequential bath perfusion with normal PSS, after addition of 0·1 mM $CdCl_2$ and then the further addition of 2 mM $BaCl_2$. The times at which current records shown in *C* were obtained are indicated by *a*, *b*, *c*.

TEA block of the steady-state outward K^+ current was accompanied by an increase in the rate of activation. The half-times ($t_{\frac{1}{2}}$) for activation of the total and Cd^{2+}-insensitive K^+ currents were reduced by 7 and 25%, respectively, in the presence of 1 mM TEA. Further increase of the external [TEA] decreased activation $t_{\frac{1}{2}}$.

In an attempt to separate I_{Kv} and I_{KCa}, the effect of charybdotoxin (CTX), an antagonist of the large conductance, Ca^{2+}-activated K^+ channel (Miller, Moczydlowski, Latorre & Philipps, 1985), was examined on the outward K^+ currents in these neurones. Bath application of CTX (100 nM) inhibited the total outward current by ~ 35% at all voltages as shown in Fig. 10*A*. The remaining K^+ current was not further reduced by the addition of 0·1 mM Cd^{2+} to the external solution (Fig.

10*B*). Similar results were obtained in three cells and this suggests that 100 nM CTX selectively inhibits I_{KCa} in rat parasympathetic neurones.

Figure 11*A* shows that the total delayed I_K was also inhibited by the addition of 0·3 and 1 mM 4-AP to the extracellular solution. Increasing the [4-AP] to 10 mM had no additional effect on current amplitude. Similar results were obtained in three additional neurones. The activation of I_K was slowed by increasing the 4-AP concentration. Bath application of 1 mM 4-AP reduced the K^+ current evoked by depolarization to +90 mV by 29% and increased $\tau_{\frac{1}{2}}$ 2·8-fold.

Both components of the delayed K^+ current, I_{Kv} and I_{KCa}, were inhibited by external Ba^{2+}. Figure 11*C* shows K^+ current amplitudes measured before and during exposure to Cd^{2+} and Ba^{2+}. Bath application of 0·1 mM Cd^{2+} reduced K^+ current amplitude by ~45% by inhibiting I_{KCa}, and the addition of 2 mM Ba^{2+} further reduced the amplitude of the K^+ current (I_{Kv}) to 17% of control (Fig. 11*D*). External Ba^{2+} alone inhibited both I_{KCa} and I_{Kv} reversibly.

DISCUSSION

In this study we have described the ionic currents contributing to the resting membrane potential and characterized voltage- and Ca^{2+}-dependent K^+ currents of cultured neurones dissociated from rat intracardiac ganglia.

Resting membrane potential

The resting membrane potential of rat parasympathetic cardiac neurones ranged between −45 and −65 mV (mean = −52 ± 2·1 mV), which is similar to that reported for rat sympathetic neurones (−54·9 ± 4·6 mV; Schofield & Ikeda, 1989), frog parasympathetic cardiac neurones (−55·4 ± 1·1 mV; Clark *et al.* 1990) and cultured intracardiac neurones from guinea-pig atria (−45 to −76 mV; Allen & Burnstock, 1987). The resting membrane potential is established primarily by a resting K^+ conductance, since the membrane potential shifted in response to changes in the extracellular [K^+]. However, the relationship between the extracellular [K^+] and resting membrane potential deviated from that predicted by the Nernst equation for a purely K^+-selective electrode, suggesting that the membrane potential is not determined solely by a resting K^+ permeability. The membrane permeability to Na^+, with a P_{Na}/P_K of 0·12, also contributes to the resting membrane potential and probably accounts for the difference of the membrane potential from the calculated E_K (−85 mV). The observed hyperpolarization of the neurone and concomitant decrease in holding current at −70 mV upon replacement of extracellular Na^+ with arginine is consistent with a resting Na^+ permeability.

The whole-cell *I–V* relation obtained by voltage ramp suggests that a voltage-insensitive leakage current and a voltage-dependent outward K^+ current are activated at the resting membrane potential (Fig. 3*A*), both of which may play roles in maintaining the resting membrane potential. Under our experimental conditions, the resting membrane potential appeared to be determined primarily by the delayed K^+ conductance, an idea consistent with the significant steady-state K^+ current around the resting potential suggested by the considerable overlap between the activation and steady-state inactivation curves of the delayed K^+ conductance (Fig.

8). Contribution of a delayed K^+ conductance to the resting membrane potential is further supported by the depolarization observed with bath application of the K^+ channel blockers, TEA and Ba^{2+}, and the lack of effect of Cl^--free solutions and Na^+–K^+ pump inhibition on the resting membrane potential. Unlike mammalian sympathetic neurones (Christ & Nishi, 1973; Freschi, 1983; Cassell, Clark & McLachlan, 1986), rat parasympathetic cardiac neurones showed no evidence of an inwardly rectifying K^+ channel. A leakage current, a voltage-sensitive delayed rectifier K^+ current and an M-current have been proposed to control the resting membrane potential in bullfrog sympathetic neurones (Adams, Brown & Constanti, 1982*a*). However, a recent study in frog sympathetic neurones reported that a relatively voltage-insensitive leakage current is primarily responsible for determining their resting membrane potential (Jones, 1989).

Action potential

The characteristics of the action potential and after-hyperpolarization in rat parasympathetic cardiac neurones are similar to those described for rat sympathetic (Schofield & Ikeda, 1989) and frog parasympathetic cardiac neurones (Clark *et al.* 1990). They are also similar to those recorded from rat cardiac neurones *in situ* (Seabrook *et al.* 1990). Two types of firing patterns were observed in cultured rat cardiac neurones with sustained depolarization: a single action potential was evoked in 85% of the cells regardless of stimulus intensity or duration, and repetitive firing could be elicited in the remaining 15% of the cells. These responses are consistent with the intracellular microelectrode recording of electrical activity in two (AH_s and AH_m) of three types of cultured neurones from guinea-pig heart (Allen & Burnstock, 1987).

The repolarization phase of the action potential and the slow after-hyperpolarization are due to the activation of the delayed outward K^+ current, which consists of at least two components: the Ca^{2+}-dependent K^+ current, I_{KCa}, and the Ca^{2+}-insensitive delayed rectifier K^+ current, I_{Kv}. Inhibition of the K^+ currents with TEA increased the action potential duration and inhibited the slow after-hyperpolarization. The reduction of the after-hyperpolarization by Cd^{2+} and further inhibition on addition of TEA suggests differential roles of the Ca^{2+}-activated K^+ current and the delayed rectifier K^+ current in the shape of the action potential and the slow after-hyperpolarization.

Depolarization-activated K^+ currents

Table 2 summarizes K^+ conductances described in various autonomic neurones, to allow comparison between the rat parasympathetic neurones described here and other autonomic ganglion cells. The Ca^{2+}-dependent K^+ current accounted for approximately 35% of the total outward K^+ current observed in rat parasympathetic cardiac neurones. Its activation kinetics are similar to those of the delayed rectifier K^+ current and similarly is reversibly inhibited by TEA and Ba^{2+}. Ca^{2+}-dependent K^+ currents have been described in rat sympathetic neurones (Freschi, 1983; Galvan & Sedlmeir, 1984; Belluzzi, Sacchi & Wanke, 1985*b*; Marrion, Smart & Brown, 1987; Schofield & Ikeda, 1989; Belluzzi & Sacchi, 1990), and in frog sympathetic (Adams, Constanti, Brown & Clark, 1982*b*; MacDermott & Weight, 1982; Pennefather,

Lancaster, Adams & Nicoll, 1985; Adams & Galvan, 1986) and parasympathetic neurones (Clark *et al.* 1990). The Ca^{2+}-dependent K^+ current in rat parasympathetic cardiac neurones contributes to the after-hyperpolarization (Fig. 4*D*). The after-hyperpolarization in cultured intracardiac neurones of the guinea-pig has also been shown to be attenuated by removal of extracellular Ca^{2+} or addition of Cd^{2+} to the extracellular solution (Allen & Burnstock, 1987).

TABLE 2. Potassium currents in autonomic ganglion cells

K^+ current	Rat parasympathetic[a]	Rat Sympathetic	Frog parasympathetic[b]
I_{Kv}	+	+[d–f,h]	+
I_{KCa}	+	+[d–h]	+
I_{AHP}	?	+[c]	—
I_A	—	+[c–g]	—
I_M	+	+[c,j]	—
I_{Ki}	—	+[d]	—

Abbreviations: I_{Kv}, delayed rectifier K^+ current; I_{KCa}, fast Ca^{2+}-activated K^+ current; I_{AHP}, slow Ca^{2+}-activated K^+ current; I_A, A-current; I_M, M-current; I_{Ki}, inward rectifier K^+ current.

References: [a] Present study; [b] Clark *et al.* 1990; [c] Marrion *et al.* 1987; [d] Freschi, 1983; [e] Galvan & Sedlmeir, 1984; [f] Belluzzi *et al.* 1985*b*; [g] Belluzzi & Sacchi, 1990; [h] Schofield & Ikeda, 1989; [i] Belluzzi *et al.* 1985*a*; [j] Constanti & Brown, 1981.

The Cd^{2+}-resistant delayed rectifier K^+ current in rat parasympathetic neurones exhibits voltage-dependent and pharmacological properties similar to those of the delayed rectifier K^+ current found in rat sympathetic neurones (Freschi, 1983; Galvan & Sedlmeir, 1984; Belluzzi *et al.* 1985*b*) and frog sympathetic and parasympathetic neurones (Adams *et al.* 1982*a*; Adams & Galvan, 1986; Lancaster & Pennefather, 1987; Clark *et al.* 1990). In rat parasympathetic cardiac neurones this current contributes to maintaining the resting membrane potential, and probably contributes to the repolarization phase of the action potential, since it is the major component of the depolarization-activated whole-cell K^+ current. The transient outward (A-current) and inwardly rectifying K^+ currents which have been described in rat sympathetic neurones (Freschi, 1983; Galvan & Sedlmeir, 1984; Belluzzi *et al.* 1985*a*; Schofield & Ikeda, 1989) were not detectable in cultured rat parasympathetic cardiac neurones. Although a muscarine-sensitive, non-inactivating K^+ current (I_M; Brown & Adams, 1980) was not investigated in the present study, a slow, long-lasting inward current evoked upon pressure application of acetylcholine or muscarine to the soma has been observed in these neurones (D. J. Adams, unpublished observations).

Mammalian parasympathetic cardiac ganglia receive preganglionic input from vagal nerve fibres and help control cardiac function and parasympathetic tone in the heart. The time- and voltage-dependent properties of the K^+ conductances in rat intracardiac neurones influence neuronal excitability by affecting both the resting membrane potential and action potential duration and frequency. Mammalian parasympathetic neurones have distinct electrophysiological characteristics which may underlie complex integrative and regulatory functions within cardiac ganglia.

We thank Drs Ellen Barrett, Wolfgang Nonner and Thomas Nutter for their constructive criticisms of a draft of this manuscript. This work was supported by National Institutes of Health grant HL 35422 to D. J. Adams.

REFERENCES

ADAMS, P. R., BROWN, D. A. & CONSTANTI, A. (1982*a*). M-currents and other potassium currents in bullfrog sympathetic neurones. *Journal of Physiology* **330**, 537–572.

ADAMS, P. R., CONSTANTI, A., BROWN, D. A. & CLARK, R. B. (1982*b*). Intracellular Ca^{2+} activates a fast voltage-sensitive K^+ current in vertebrate sympathetic neurones. *Nature* **296**, 746–749.

ADAMS, P. R. & GALVAN, M. (1986). Voltage-dependent currents on vertebrate neurones and their role in membrane excitability. *Advances in Neurology* **44**, 137–170.

ALLEN, T. G. J. & BURNSTOCK, G. (1987). Intracellular studies of the electrophysiological properties of cultured intracardiac neurones of the guinea-pig. *Journal of Physiology* **388**, 349–366.

ARMOUR, J. A. & HOPKINS, D. A. (1990). Activity of canine in situ left atrial ganglion neurones. *American Journal of Physiology* **259**, H1207–1215.

BELLUZZI, O. & SACCHI, O. (1990). The calcium-dependent potassium conductance in rat sympathetic neurones. *Journal of Physiology* **422**, 561–583.

BELLUZZI, O., SACCHI, O. & WANKE, E. (1985*a*). A fast transient outward current in the rat sympathetic neurones studied under voltage-clamp conditions. *Journal of Physiology* **358**, 91–108.

BELLUZZI, O., SACCHI, O. & WANKE, E. (1985*b*). Identification of delayed potassium and calcium current in the rat sympathetic neurone under voltage clamp. *Journal of Physiology* **358**, 109–129.

BROWN, D. A. & ADAMS, P. R. (1980). Muscarinic suppression of novel voltage-sensitive K^+ current in a vertebrate neurones. *Nature* **283**, 673–676.

CASSELL, J. F., CLARK, A. L. & MCLACHLAN, E. M. (1986). Characteristics of phasic and tonic sympathetic ganglion cells of the guinea-pig. *Journal of Physiology* **372**, 457–483.

CHRIST, D. D. & NISHI, S. (1973). Anomalous rectification of mammalian sympathetic ganglion cells. *Experimental Neurology* **40**, 806–815.

CLARK, R. B., TSE, A. & GILES, W. R. (1990). Electrophysiology of parasympathetic neurones isolated from the interatrial septum of bull-frog heart. *Journal of Physiology* **427**, 89–125.

CONSTANTI, A. & BROWN, D. A. (1981). M-current in voltage-clamped mammalian sympathetic neurones. *Neuroscience Letters* **24**, 289–294.

DENNIS, M. J., HARRIS, A. J. & KUFFLER, S. W. (1971). Synaptic transmission and its duplication by focally applied acetylcholine in parasympathetic neurones in the heart of the frog. *Proceedings of the Royal Society* B **177**, 509–539.

ELLISON, J. P. & HIBBS, R. G. (1976). An ultrastructural study of mammalian cardiac ganglia. *Journal of Molecular and Cellular Cardiology* **8**, 89–101.

FIEBER, L. A. & ADAMS, D. J. (1991). Acetylcholine-evoked currents in cultured neurones dissociated from rat parasympathetic cardiac ganglia. *Journal of Physiology* **434**, 215–237.

FRESCHI, J. E. (1983). Membrane currents of cultured rat sympathetic neurons under voltage clamp. *Journal of Neurophysiology* **50**, 1460–1478.

GAGLIARDI, M., RANDALL, W. C., BIEGER, D., WURSTER, R. D., HOPKINS, D. A. & ARMOUR, J. A. (1988). Activity of in vivo canine cardiac plexus neurons. *American Journal of Physiology* **255**, H789–800.

GALVAN, M. & SEDLMEIR, C. (1984). Outward currents in voltage-clamped rat sympathetic neurones. *Journal of Physiology* **356**, 115–133.

GOLDMAN, D. E. (1943). Potential, impedance, and rectification in membranes. *Journal of General Physiology* **27**, 37–60.

HAMILL, O. P., MARTY, A., NEHER, E., SAKMANN, B. & SIGWORTH, F. J. (1981). Improved patch-clamp techniques for high resolution current recording from cells and cell-free membrane patches. *Pflügers Archiv* **391**, 85–100.

HODGKIN, A. L. & KATZ, B. (1949). The effect of sodium ions on the electrical activity of the giant axon of the squid. *Journal of Physiology* **108**, 37–77.

JONES, S. W. (1989). On the resting potential of isolated frog sympathetic neurones. *Neuron* **3**, 153–161.

KING, T.-S. & COAKLEY, J. B. (1958). The intrinsic nerve cells of the cardiac atria of mammals and man. *Journal of Anatomy* **92**, 353–379.

LANCASTER, B. & PENNEFATHER, P. (1987). Potassium currents evoked by brief depolarizations in bull-frog sympathetic ganglion cells. *Journal of Physiology* **387**, 519–548.

MacDermott, A. B. & Weight, F. F. (1982). Action potential repolarization may involve a transient, Ca^{2+}-sensitive outward current in a vertebrate neurone. *Nature* **300**, 185–188.

Marrion, N. V., Smart, T. G. & Brown, D. A. (1987). Membrane currents in adult rat superior cervical ganglia in dissociated tissue culture. *Neuroscience Letters* **77**, 55–60.

Meiklejohn, J. (1914). On the topography of the intra-cardiac ganglia of the rat's heart. *Journal of Anatomy and Physiology* **48**, 378–381.

Miller, C., Moczydlowski, E., Latorre, R. & Philipps, M. (1985). Charybdotoxin, a protein inhibitor of single Ca^{2+}-activated K^+ channels from mammalian skeletal muscle. *Nature* **313**, 316–318.

Moravec, M. & Moravec, J. (1984). Intrinsic innervation of the atrioventricular junction of the rat heart. *American Journal of Anatomy* **171**, 307–319.

Nozdrachev, A. D. & Pogorelov, A. G. (1982). Extracellular recording of neuronal activity of the cat heart ganglia. *Journal of the Autonomic Nervous System* **6**, 73–81.

Pardini, B. J., Patel, K. P., Schmid, P. G. & Lund, D. D. (1987). Location, distribution and projections of intracardiac ganglion cells in the rat. *Journal of the Autonomic Nervous System* **20**, 91–101.

Pennefather, P., Lancaster, B., Adams, P. R. & Nicoll, R. A. (1985). Two distinct Ca^{2+}-dependent K currents in bullfrog sympathetic ganglion cells. *Proceedings of the National Academy of Sciences of the USA* **82**, 3040–3044.

Roper, S. (1976). An electrophysiological study of chemical and electrical synapses on neurones in the parasympathetic cardiac ganglion of the mudpuppy, *Necturus maculosus*: evidence for intrinsic ganglionic innervation. *Journal of Physiology* **254**, 427–454.

Schofield, G. G. & Ikeda, S. R. (1989). Potassium currents of acutely isolated adult rat superior cervical ganglion neurones. *Brain Research* **485**, 205–214.

Seabrook, G. R., Fieber, L. A. & Adams, D. J. (1990). Neurotransmission in neonatal rat cardiac ganglion in situ. *American Journal of Physiology* **259**, H997–1005.

Woollard, H. H. (1926). The innervation of the heart. *Journal of Anatomy* **60**, 345–373.

Xi, X., Thomas, J. X., Randall, W. C. & Wurster, R. D. (1991). Intracellular recordings from canine intracardiac ganglion cells. *Journal of the Autonomic Nervous System* **32**, 177–182.

Xu, Z.-J. & Adams, D. J. (1992). Voltage-dependent sodium and calcium currents in cultured parasympathetic neurones from rat intracardiac ganglia. *Journal of Physiology* **456**, 425–441.